

The Gas Accretion Rate of Galaxies over $z \approx 0 - 1.3$

ADITYA CHOWDHURY,¹ NISSIM KANEKAR,¹ AND JAYARAM N. CHENGALUR¹

¹National Centre for Radio Astrophysics, Tata Institute of Fundamental Research, Pune, India.

ABSTRACT

We present here estimates of the average rates of accretion of neutral gas onto main-sequence galaxies and the conversion of atomic gas to molecular gas in these galaxies at two key epochs in galaxy evolution: (i) $z \approx 1.3 - 1.0$, towards the end of the epoch of peak star-formation activity in the Universe, and (ii) $z \approx 1 - 0$, when the star-formation activity declines by an order of magnitude. We determine the net gas accretion rate R_{Acc} and the molecular gas formation rate R_{Mol} by combining the relations between the stellar mass and the atomic gas mass, the molecular gas mass, and the star-formation rate (SFR) at three epochs, $z = 1.3$, $z = 1.0$, and $z = 0$, with the assumption that galaxies evolve continuously on the star-forming main-sequence. We find that, for all galaxies, R_{Acc} is far lower than the average SFR R_{SFR} at $z \approx 1.3 - 1.0$; however, R_{Mol} is similar to R_{SFR} during this interval. Conversely, both R_{Mol} and R_{Acc} are significantly lower than R_{SFR} over the later interval, $z \approx 1 - 0$. We find that massive main-sequence galaxies had already acquired most of their present-day baryonic mass by $z \approx 1.3$. At $z \approx 1.3 - 1.0$, the rapid conversion of the existing atomic gas to molecular gas was sufficient to maintain a high average SFR, despite the low net gas accretion rate. However, at later times, the combination of the lower net gas accretion rate and the lower molecular gas formation rate leads to a decline in the fuel available for star-formation, and results in the observed decrease in the SFR density of the Universe over the last 8 Gyr.

Keywords: Galaxy evolution — Neutral hydrogen clouds — High- z galaxies

1. INTRODUCTION

The evolution of galaxies is driven by the baryon cycle in which the baryonic constituents of galaxies and their circumgalactic mediums (CGMs) interact with each other and convert from one form to another (e.g. Péroux & Howk 2020). The key processes in the baryon cycle are (i) the accretion of mostly ionized gas from the CGM onto the “disks” of galaxies, forming neutral atomic hydrogen (HI) in the disks, (ii) the cooling of HI and its conversion to molecular hydrogen (H₂), (iii) the gravitational collapse and fragmentation of molecular clouds to form stars, and (iv) the expulsion of gas from the interstellar mediums (ISMs) of galaxies in outflows driven by stars or active galactic nuclei (AGNs), with some fraction of this gas later returning to the galaxy disk.

Measurements of the rates at which the above processes occur in galaxies, how the rates compare to each other, and how they evolve with redshift are critical to understanding galaxy evolution. Unfortunately, only the redshift evolution

of the stellar properties of galaxies and their star-formation rates (SFR) are well determined today. For example, we have known for over two decades that the SFR density of the Universe peaks in the redshift range $z \approx 1 - 3$ and then declines by an order of magnitude from $z \approx 1$ to $z \approx 0$ (e.g. Madau & Dickinson 2014). Further, $\approx 90\%$ of the star-formation activity of the Universe out to $z \approx 2$ occurs on the “star-forming main sequence” (e.g. Rodighiero et al. 2011) — a tight relationship between the SFR and the stellar mass (M_*) of galaxies (e.g. Noeske et al. 2007; Whitaker et al. 2014). At a fixed stellar mass, the SFR of galaxies on the main sequence declines by a factor of ≈ 10 from $z \approx 1$ to the present time (e.g. Whitaker et al. 2014; Popesso et al. 2022).

Unlike the SFR of a galaxy, it is very challenging to observationally determine the gas accretion rate and the rate at which HI is converted to H₂. While there have been suggestions in the literature that a low gas accretion rate at late times might account for various observational results (e.g. Bouché et al. 2010; Møller et al. 2013; Walter et al. 2020; Chowdhury et al. 2020), the lack of actual measurements of the accretion rate has been a key limitation in our understanding of the processes that drive the redshift evolution of the star-formation activity of the Universe. For example, Walter et al. (2020)

used the redshift evolution of the cosmological SFR density, the cosmological HI mass density, and the cosmological H₂ mass density to estimate the rate of global flow of gas, and global conversion of HI to H₂. However, such global rates, averaged over cosmological volumes, are difficult to interpret and do not provide any information on the differences between different galaxy populations, such as the dependence of the accretion rate on galaxy stellar mass, environment, morphology, etc. Conversely, [Bouché et al. \(2010\)](#) used a toy “reservoir” model, in which gas accretion is quenched above a halo mass of $\approx 10^{11} M_{\odot}$, to argue that the decline in SFR density from $z \approx 2$ may be driven by the decline in the gas accretion rate. This model was found to yield the observed main-sequence and Tully-Fisher scaling relations at different redshifts (see also [Møller et al. 2013](#), for the mass-metallicity relation). However, its predicted gas fractions ($\approx 30\text{--}45\%$ at $z \approx 1.2$) are lower than the values recently measured ($\approx 80\%$ at $z \approx 1.3$) by [Chowdhury et al. \(2022a\)](#).

The net gas accretion rate (i.e. the difference between the gas inflow and outflow rates) and the H₂ formation rate can be determined if one knows the dependences of the HI and H₂ masses of galaxies on their stellar masses (i.e. the $M_{\text{HI}} - M_{*}$ and $M_{\text{Mol}} - M_{*}$ scaling relations; [Scoville et al. 2017](#); [Bera et al. 2023a](#)), along with the standard assumption that star-forming galaxies evolve along the main sequence (e.g. [Renzini 2009](#); [Peng et al. 2010](#); [Leitner 2012](#); [Speagle et al. 2014](#); [Scoville et al. 2017](#)). For the molecular component, various observational tracers (primarily CO rotational lines and dust continuum emission) have been used to determine the $M_{\text{Mol}} - M_{*}$ relation of galaxies out to $z \approx 5$ (e.g. [Tacconi et al. 2020](#)). However, the weakness of the HI 21 cm line, the only tracer of the HI mass of galaxies, has meant that, until very recently, estimates of the $M_{\text{HI}} - M_{*}$ relation were limited to the local Universe (e.g. [Catinella et al. 2018](#); [Parkash et al. 2018](#)).

The HI 21 cm stacking approach, based on combining the HI 21 cm emission signals from a large number of galaxies with accurately known positions and redshifts, allows one to overcome the intrinsic weakness of the HI 21 cm line and measure the average HI properties of galaxy populations at cosmological distances ([Zwaan 2000](#); [Chengalur et al. 2001](#)). This approach has been recently used to measure the HI properties of star-forming galaxies out to $z \approx 1$ (e.g. [Bera et al. 2019, 2022, 2023b](#); [Chowdhury et al. 2020, 2021, 2022b](#)). Recently, [Chowdhury et al. \(2022c\)](#) applied the HI 21 cm stacking approach to data from the Giant Metrewave Radio Telescope (GMRT) Cold-HI AT $z \approx 1$ (CAT z 1) survey, a 510-hr HI 21 cm emission survey of galaxies at $z = 0.74 - 1.45$ ([Chowdhury et al. 2022b](#)), to obtain the first measurement of the $M_{\text{HI}} - M_{*}$ scaling relation at $z \approx 1$.

In this Letter, we combine measurements of the $M_{\text{HI}} - M_{*}$ scaling relation at $z \approx 1$ from the GMRT-CAT z 1 survey with

estimates of the star-forming main-sequence relation and the $M_{\text{Mol}} - M_{*}$ scaling relation from the literature, and the assumption of the continuity of galaxy evolution along the main sequence, to determine the average H₂ formation rate and the average net gas accretion rate in star-forming galaxies over the redshift intervals $z \approx 1.3 - 1.0$ and $z \approx 1.0 - 0$.

Throughout this work, we assume a Chabrier initial mass function (IMF) for estimates of the stellar masses and SFRs. Further, we use a flat Lambda-cold dark matter cosmology, with $\Omega_m = 0.3$, $\Omega_{\Lambda} = 0.7$, and $H_0 = 70 \text{ km s}^{-1} \text{ Mpc}^{-1}$.

2. DETERMINATION OF THE GAS ACCRETION RATE AND THE H₂ FORMATION RATE

2.1. Formalism

The formalism used in this work to determine the net gas accretion rate and the H₂ formation rate of star-forming galaxies was introduced by [Scoville et al. \(2017\)](#), and recently refined by [Bera et al. \(2023a\)](#) to include the $M_{\text{HI}} - M_{*}$ relation. In this approach, the build-up of the stellar mass of a galaxy, with an initial stellar mass ($M_{*,i}$) at the initial epoch (t_i), is tracked to determine the final stellar mass ($M_{*,f}$) at the final epoch (t_f). This is done by assuming that the galaxy remains on the star-forming main-sequence over the entire period, such that

$$M_{*,f} = M_{*,i} + \int_{t_i}^{t_f} (1 - f_{\text{return}}) \text{SFR}_{\text{MS}}(M_{*}, t) dt \quad (1)$$

where $\text{SFR}_{\text{MS}}(M_{*}, t)$ is the main-sequence relation at the time t , and f_{return} is the fraction of the stellar mass returned to the ISM via stellar winds or supernovae ($f_{\text{return}} = 0.41$ for a Chabrier IMF; [Leitner & Kravtsov 2011](#); [Madau & Dickinson 2014](#)). We define here the average star-formation rate R_{SF} between the epochs t_i and t_f , such that

$$M_{*,f} = M_{*,i} + (1 - f_{\text{return}}) R_{\text{SF}} \Delta t \quad (2)$$

where $\Delta t = t_f - t_i$ is the time interval between the two epochs of interest. Measurements of the star-forming main-sequence (e.g. [Whitaker et al. 2014](#); [Popesso et al. 2022](#)) can then be used to track the evolution of the stellar mass of a main-sequence galaxy using Equation 1, and this can be combined with Equation 2 to determine R_{SF} using the following relation.

$$R_{\text{SF}} = \frac{(M_{*,f} - M_{*,i})}{(1 - f_{\text{return}}) \Delta t} \quad (3)$$

Next, the final molecular gas reservoir¹, $M_{\text{Mol},f}$, of the galaxy at time t_f is related to the initial molecular gas reservoir, $M_{\text{Mol},i}$, at time t_i via

$$M_{\text{Mol},f} = M_{\text{Mol},i} - R_{\text{SF}} \Delta t + R_{\text{Mol}} \Delta t \quad (4)$$

¹ Throughout this Letter, M_{Mol} and M_{Atom} are used to refer to gas masses that include the mass contribution of Helium

where R_{Mol} is the average molecular gas formation rate between the two epochs of interest, i.e. the difference between the rate at which HI is converted to H_2 and that at which H_2 is dissociated to HI. Given that the initial and final stellar masses are known, one can use measurements of the molecular gas mass as a function of stellar mass at both epochs to determine $M_{\text{Mol},f}$ and $M_{\text{Mol},i}$ which can then be combined with Equation 4 to obtain R_{Mol} using the following relation.

$$R_{\text{Mol}} = R_{\text{SF}} + (M_{\text{Mol},f} - M_{\text{Mol},i})/\Delta t \quad (5)$$

Finally, the neutral atomic gas mass, $M_{\text{Atom},f}$, of the galaxy at time t_f is related to the initial neutral atomic gas mass, $M_{\text{Atom},i}$, at time t_i via the relation

$$M_{\text{Atom},f} = M_{\text{Atom},i} - R_{\text{Mol}}\Delta t + R_{\text{Acc}}\Delta t \quad (6)$$

where R_{Acc} is the *net* accretion rate of neutral atomic gas onto the disk of the galaxy, i.e. the difference between the neutral atomic gas inflow and outflow rates. Again, measurements of M_{HI} as a function of stellar mass at the two epochs can be used to determine $M_{\text{Atom},f}$ and $M_{\text{Atom},i}$, which can be combined with Equation 6 to obtain R_{Acc} using the following relation:

$$R_{\text{Acc}} = R_{\text{Mol}} + (M_{\text{Atom},f} - M_{\text{Atom},i})/\Delta t \quad (7)$$

We note that in the above formalism, the stellar mass returned to the ISM is assumed to be mostly in the ionised state and is hence not explicitly included in Equations 4-7. It is entirely possible that some fraction of this gas cools to form HI or H_2 over the time interval between t_i and t_f . However, we emphasize that even assuming that *all* of the stellar mass that is returned to the ISM cools to form HI would not significantly alter the key conclusions of this work.

We use the above formalism to estimate R_{SF} , R_{Mol} , and R_{Acc} over two redshift intervals: (a) $z \approx 1.3$ to $z \approx 1.0$, covering the end of the epoch of peak cosmic star-formation activity, and (b) $z \approx 1.0$ to $z \approx 0$, covering the decline of star-formation activity over the last ≈ 8 Gyr (e.g. [Madau & Dickinson 2014](#)). The choice of these redshift intervals is driven by our recent measurements of the average HI content of stellar mass-matched samples of star-forming galaxies at $z \approx 1.0$ and $z \approx 1.3$ ([Chowdhury et al. 2022d](#)), and the measurement of the $M_{\text{HI}} - M_*$ scaling relation over the redshift range $0.74 \leq z \leq 1.45$ ([Chowdhury et al. 2022c](#)). In the following subsections, we briefly describe the relations that were used to estimate SFR, M_{Mol} , and M_{Atom} for star-forming galaxies at $z \approx 1.3$, $z \approx 1.0$, and $z \approx 0$, specifically (i) the star-forming main-sequence relation (e.g. [Whitaker et al. 2014](#); [Popesso et al. 2022](#)), (ii) the $M_{\text{Mol}} - M_*$ relation ([Tacconi et al. 2020](#)), and (iii) the $M_{\text{HI}} - M_*$ relation ([Catinella et al. 2018](#); [Chowdhury et al. 2022c](#)).

2.2. The Star-Forming Main-Sequence

We use the star-forming main-sequence relation of [Popesso et al. \(2022\)](#) to estimate the build-up of the stellar mass of galaxies via Equation 1. These authors converted a large number of literature measurements of the main sequence at $0 < z < 6$ to a common calibration, to find that the data are consistent with a relation that is linear at low stellar masses and flattens above a characteristic stellar mass (see also [Whitaker et al. 2014](#)). We will use the following main-sequence relation, obtained via a second-order polynomial fit to the dependence of $\log[\text{SFR}]$ on $\log[M_*]$ ([Popesso et al. 2022](#)):

$$\log[\text{SFR}(M_*, t)] = (a_1 t + b_1) \log[M_*] + b_2 \log^2[M_*] + (b_0 + a_0 t) \quad (8)$$

where t is the age of the Universe at the epoch of interest and the fit parameters are $a_0 = 0.20 \pm 0.02$, $a_1 = -0.034 \pm 0.002$, $b_0 = -26.134 \pm 0.015$, $b_1 = 4.722 \pm 0.012$, and $b_2 = -0.1925 \pm 0.0011$ ([Popesso et al. 2022](#)). The main-sequence relations at $z \approx 0$, $z \approx 1.0$, and $z \approx 1.3$, obtained using Equation 8, are shown as the solid blue curves in Figure 1[A].

In passing, we emphasize that the main conclusions of this work are unchanged on using the second main-sequence relation of [Popesso et al. \(2022\)](#), which asymptotically approaches a maximum SFR value with increasing stellar mass, or the main-sequence relation of [Whitaker et al. \(2014\)](#), which is commonly used in the literature.

2.3. The $M_{\text{Mol}} - M_*$ Relation

For the $M_{\text{Mol}} - M_*$ relation, we follow [Tacconi et al. \(2020\)](#), who compiled literature estimates of the molecular gas mass of 2052 galaxies with $M_* \approx 10^9 - 10^{11.5} M_\odot$ at $0 \lesssim z \lesssim 5.2$. The molecular gas masses were estimated using different tracers such as the CO rotational lines (e.g. [Daddi et al. 2010](#); [Tacconi et al. 2013](#); [Saintonge et al. 2017](#)), the far-infrared dust continuum (e.g. [Santini et al. 2014](#)), and the 1 mm dust continuum (e.g. [Scoville et al. 2016](#)). [Tacconi et al. \(2020\)](#) corrected the measurements obtained from the different tracers for any zero-point offsets, to put them on the same scale, and obtained the following relation for the dependence of the molecular gas mass of main-sequence galaxies on redshift and stellar mass:²

$$\log \left[\frac{M_{\text{Mol}}}{M_*} \right] = A + B [\log(1+z) - F]^2 + D [\log M_* - 10.7] \quad (9)$$

² We note that the relation in [Tacconi et al. \(2020\)](#) also includes a term giving the dependence on the offset from the main-sequence relation. We have dropped this term as our study is restricted to galaxies lying on the main sequence.

where the coefficients $A = 0.06 \pm 0.2$, $B = -3.33 \pm 0.2$, $F = 0.65 \pm 0.05$, and $D = -0.41 \pm 0.03$ (note that the quoted uncertainties are 2σ errors; Tacconi et al. 2020). We will use Equation 9 to determine the $M_{\text{Mol}} - M_*$ relation at $z \approx 0$, $z \approx 1.0$, and $z \approx 1.3$; these scaling relations are shown as the solid blue lines in Figure 1[B].

2.4. The $M_{\text{Atom}} - M_*$ Relation

We determine the $M_{\text{HI}} - M_*$ relation at $z \approx 1.0$ and $z \approx 1.3$ from the measurements of the average HI mass of main-sequence galaxies at these redshifts in the GMRT-CATz1 survey (Chowdhury et al. 2022b). This survey covered the HI 21 cm line of 11,419 main-sequence galaxies at $z = 0.74 - 1.45$ with stellar masses $M_* = 10^9 - 10^{11.5} M_\odot$. Chowdhury et al. (2022c) divided the sample of 11,419 galaxies into three stellar-mass subsamples, and measured the average HI mass of the galaxies in each subsample, and fitted a linear relation to the M_{HI} and M_* estimates to determine the $M_{\text{HI}} - M_*$ relation at $z \approx 1$. They found that the slope of the $M_{\text{HI}} - M_*$ relation at $z \approx 1$ is consistent with that at $z \approx 0$. However, the intercept of the relation at $z \approx 1$ is higher than that of the local relation by a factor of ≈ 3.5 .

Chowdhury et al. (2022c) also determined the $M_{\text{HI}} - M_*$ relation for blue ($\text{NUV}-r < 4$) galaxies at $z \approx 0$ from M_{HI} measurements of galaxies covered in the extended GALEX Arcicbo Sloan Digital Sky Survey (xGASS; Catinella et al. 2018): xGASS is an Arcicbo telescope HI 21 cm survey of a sample of stellar mass-selected galaxies at $z \approx 0$, with stellar masses in the range $10^{9.0} - 10^{11.5} M_\odot$. They obtained the relation $\log[M_{\text{HI}}] = (0.38 \pm 0.05) \log[M_{*,10}] + (9.634 \pm 0.019)$, where $M_{*,10} = \log[M_*/10^{10} M_\odot]$. Since the slope of the $M_{\text{HI}} - M_*$ relation for the GMRT-CATz1 galaxies at $z \approx 0.74 - 1.45$ is the same as that of the relation at $z \approx 0$, we will assume that the slope of the $M_{\text{HI}} - M_*$ relation is constant, and equal to 0.38 (i.e. the xGASS slope), over the entire redshift range $z \approx 0 - 1.3$.

Next, Chowdhury et al. (2022d) subdivided the DEEP2 galaxies into two redshift bins, at $0.74 < z \leq 1.25$ and $1.25 < z \leq 1.45$, to measure the average HI mass of main-sequence galaxies at average redshifts of $\langle z \rangle \approx 1$ and $\langle z \rangle \approx 1.3$. They obtained average HI masses of $\langle M_{\text{HI}} \rangle = (3.36 \pm 0.64) \times 10^{10} M_\odot$ at $z \approx 1.3$ and $\langle M_{\text{HI}} \rangle = (1.06 \pm 0.19) \times 10^{10} M_\odot$ at $z \approx 1.0$, both for average stellar masses of $\langle M_* \rangle \approx 10^{10} M_\odot$. We determine the intercepts of the $M_{\text{HI}} - M_*$ relations at $z \approx 1$ and $z \approx 1.3$ by requiring that the relations are consistent with the above $\langle M_{\text{HI}} \rangle$ measurements for galaxies with $\langle M_* \rangle = 10^{10} M_\odot$ at each redshift. This yields the scaling relations

$$\log[M_{\text{HI}}] = 0.38 \log[M_{*,10}] + (10.063 \pm 0.082) \quad (z \approx 1) \quad (10)$$

and

$$\log[M_{\text{HI}}] = 0.38 \log[M_{*,10}] + (10.564 \pm 0.087) \quad (z \approx 1.3) \quad (11)$$

We note that the above $M_{\text{HI}} - M_*$ relations yield, at each redshift, the *mean* M_{HI} value for a distribution of galaxies at a given M_* . However, the main-sequence relation of Equation 8 and the $M_{\text{H}_2} - M_*$ relation of Equation 9 yield, respectively, the median SFR and the median M_{H_2} at a given stellar mass. For a log-normal distribution of HI masses, which is typically the case (e.g. Saintonge & Catinella 2022), the mean HI mass is different from the median HI mass. For consistency with the main-sequence and the $M_{\text{Mol}} - M_*$ relations, we hence correct our mean $M_{\text{HI}} - M_*$ relations to obtain the median $M_{\text{HI}} - M_*$ relations (e.g. Bera et al. 2022; Chowdhury et al. 2022c). Assuming that the HI masses of galaxies at $z \approx 1$ and $z \approx 1.3$ follow log-normal distributions with a scatter identical to the 0.4 dex scatter measured for the $M_{\text{HI}} - M_*$ relation at $z \approx 0$ (Catinella et al. 2018), the median $M_{\text{HI}} - M_*$ relations lie 0.184 dex lower than the corresponding mean relations. The median $M_{\text{HI}} - M_*$ scaling relations are then:

$$\log[M_{\text{HI}}] = 0.38 \log[M_{*,10}] + (9.879 \pm 0.082) \quad (z \approx 1), \quad (12)$$

and

$$\log[M_{\text{HI}}] = 0.38 \log[M_{*,10}] + (10.380 \pm 0.087) \quad (z \approx 1.3). \quad (13)$$

Finally, we also correct the above median relations for the mass contribution of helium, assuming $M_{\text{Atom}} = 1.36 M_{\text{HI}}$, to obtain

$$\log[M_{\text{Atom}}] = 0.38 \log[M_{*,10}] + A \quad (14)$$

where the values of the coefficient A are (9.583 ± 0.019) at $z \approx 0$, (10.012 ± 0.082) at $z \approx 1.0$, and (10.513 ± 0.087) at $z \approx 1.3$. The solid blue lines in Figure 1[C] show the median $M_{\text{Atom}} - M_*$ relation at $z \approx 0$, $z \approx 1.0$, and $z \approx 1.3$.

In passing, we note that, over the last two decades, different HI 21 cm surveys have measured the $M_{\text{HI}} - M_*$ scaling relation for various galaxy populations at $z \approx 0$, each with different galaxy selection criteria (e.g. Barnes et al. 2001; Giovanelli et al. 2005; Huang et al. 2012; Bothwell et al. 2013; Dénes et al. 2014; Catinella et al. 2018; Parkash et al. 2018). The scaling relations obtained from “blind” HI 21 cm surveys (e.g. Barnes et al. 2001; Giovanelli et al. 2005) are biased towards HI-rich galaxies, yielding $M_{\text{HI}} - M_*$ relations that lie above those obtained from HI 21 cm surveys of optically-selected galaxies (e.g. Huang et al. 2012; Catinella et al. 2018). The $M_{\text{HI}} - M_*$ relation at $z \approx 1$ from the GMRT-CATz1 survey, as well as the main-sequence relation and the $M_{\text{H}_2} - M_*$ relation used in this work, are all obtained from optically-selected galaxy samples. We hence chose to

use the scaling relation obtained from the blue galaxies in the optically-selected xGASS sample (Catinella et al. 2018) as the reference $M_{\text{HI}} - M_*$ relation at $z \approx 0$.

3. RESULTS

We use the formalism of Section 2.1 with the main-sequence relation (Equation 8), the $M_{\text{Mol}} - M_*$ relation (Equation 9), and the $M_{\text{Atom}} - M_*$ relation (Equation 14), to estimate R_{SF} , R_{Mol} , and R_{Acc} as a function of stellar mass over the redshift intervals $z \approx 1.3 - 1.0$ and $z \approx 1.0 - 0.0$. We emphasize that this implicitly assumes that star-forming galaxies evolve along the main sequence (e.g. Renzini 2009; Peng et al. 2010; Speagle et al. 2014; Scoville et al. 2017).

3.1. The Evolution of a Milky-Way-like Galaxy from $z \approx 1.3$ to $z \approx 0$

We illustrate the formalism of Section 2.1 for the case of a massive galaxy with $M_* = 10^{10} M_\odot$ at $z \approx 1.3$. We use Equation 1 and the main-sequence relation of Equation 8 to evolve the galaxy; the evolutionary track of the galaxy in the $\text{SFR} - M_*$ plane is shown in the red curve in Figure 1[A]. We find that the stellar mass of the galaxy increases to $\approx 2.1 \times 10^{10} M_\odot$ at $z \approx 1$. Using Equation 3, we find that the time-averaged SFR of the galaxy between $z = 1.3$ and $z = 1.0$ is $R_{\text{SF}} \approx 16 M_\odot \text{ yr}^{-1}$. We use the $M_{\text{Mol}} - M_*$ relation of Equation 9 to find that the molecular gas mass of the galaxy increases from $M_{\text{Mol}} \approx 1.2 \times 10^{10} M_\odot$ at $z = 1.3$ to $M_{\text{Mol}} \approx 1.3 \times 10^{10} M_\odot$ at $z = 1.0$. Using Equation 5, this yields a time-averaged molecular gas formation rate of $R_{\text{Mol}} \approx 17 M_\odot \text{ yr}^{-1}$, very similar to the average SFR, R_{SF} , over the same interval. Finally, we use the $M_{\text{Atom}} - M_*$ relation of Equation 14 to find that the atomic gas mass of the galaxy declines from $M_{\text{Atom}} \approx 3.3 \times 10^{10} M_\odot$ at $z = 1.3$ to $M_{\text{Atom}} \approx 1.4 \times 10^{10} M_\odot$ at $z = 1.0$. We use Equation 7 to find that the net accretion rate of the galaxy over this interval is $R_{\text{Acc}} \approx 1 M_\odot \text{ yr}^{-1}$. We thus find that the net accretion rate of a main-sequence galaxy with a stellar mass of $M_* = 10^{10} M_\odot$ at $z \approx 1.3$, over the interval $z = 1.3$ to $z = 1.0$, is far lower than both the average SFR and the molecular gas formation rate over the same period.

Following the same galaxy down to $z \approx 0$, we find that the stellar mass increases to $M_* \approx 5 \times 10^{10} M_\odot$ (similar to that of the Milky Way), while the molecular gas mass and atomic gas mass both decline, to values of $M_{\text{Mol}} \approx 2 \times 10^9 M_\odot$ and $M_{\text{Atom}} \approx 7 \times 10^9 M_\odot$, respectively, at $z = 0$. We note that these stellar, atomic, and molecular gas masses are similar to those of the Milky Way (e.g. Kalberla & Kerp 2009). Using Equations 3–7, we obtain $R_{\text{SF}} \approx 7 M_\odot \text{ yr}^{-1}$, $R_{\text{Mol}} \approx 5 M_\odot \text{ yr}^{-1}$, and $R_{\text{Acc}} \approx 4 M_\odot \text{ yr}^{-1}$ over the 8-Gyr interval from $z = 1.0$ to $z = 0$. We thus find that both R_{Mol} and R_{Acc} are lower than R_{SF} during the interval $z = 1.0$ to $z = 0$; this is unlike the situation in the interval $z = 1.3$ to

$z = 1.0$, where R_{Mol} was similar to R_{SF} . Further, both R_{SF} and R_{Mol} are significantly lower in the interval $z = 1.0 - 0$ than at $z = 1.3 - 1.0$; however, the time-averaged net gas accretion rate R_{Acc} over $z = 1.0 - 0$ is higher than that over $z = 1.3 - 1.0$.

3.2. The Net Gas Accretion and Molecular Gas Formation Rates as a Function of Stellar Mass

We apply a similar analysis to main-sequence galaxies with initial stellar masses (at $z = 1.3$) in the range $M_* \approx 10^9 - 10^{11.4} M_\odot$, similar to the range of stellar masses over which the GMRT-CATz1 survey obtained the $M_{\text{HI}} - M_*$ relation (Chowdhury et al. 2022c). Figure 2[A] shows, as a function of stellar mass at $z = 1.0$, our estimates of R_{SF} , R_{Mol} , and R_{Acc} over the interval $z = 1.3$ to $z = 1.0$, while Figure 2[B] shows the same quantities for the lower redshift interval $z = 1.0$ to $z = 0$, again plotted against the final stellar mass, at $z = 0$. We note that the confidence intervals shown in Figure 2 take into account the uncertainties in the $M_{\text{Atom}} - M_*$ relation and the $M_{\text{Mol}} - M_*$ relation, but not that in the main-sequence relation; the uncertainties in our estimates of R_{Mol} and R_{Acc} are dominated by those in the former two scaling relations.

Figure 2[A] shows that, except for the most massive galaxies, the time-averaged molecular gas formation rate is similar to the net average SFR over the higher-redshift interval $z = 1.3$ to $z = 1.0$. Both R_{SF} and R_{Mol} are $\gtrsim 10 M_\odot \text{ yr}^{-1}$ for galaxies with $M_* \gtrsim 10^{10} M_\odot$ at $z \approx 1.3$. Remarkably, Figure 2[A] also shows that R_{Acc} for main-sequence galaxies *over the entire stellar mass range* is far lower than both R_{SF} and R_{Mol} . Indeed, our estimate of R_{Acc} is consistent with no net accretion of neutral gas onto the disks of star-forming galaxies over the redshift range $z \approx 1.3$ to $z \approx 1$. This essentially implies that the HI that is consumed in molecular gas formation (and later, star-formation) is not replenished in main-sequence galaxies towards the end of the epoch of galaxy assembly.

For the most massive galaxies, with $M_* \gtrsim 10^{10.5} M_\odot$ at $z \approx 1.3$, Fig. 2[A] indicates that the net gas accretion rate is negative, i.e. that outflows dominate infall in such galaxies over the redshift range $z \approx 1.3$ to $z \approx 1.0$. Evidence has indeed been found for stronger outflows in higher stellar-mass galaxies at these redshifts: for example, Weiner et al. (2009) find that the outflow velocity in DEEP2 galaxies at $z \approx 1.4$ scales $\propto \text{SFR}^{0.3}$, implying that the outflowing material may escape from high-mass galaxies. However, we emphasize that the result that outflows dominate infall in high-mass galaxies remains tentative, due to the uncertainties in the different scaling relations.

In the lower-redshift interval ($z = 1$ to $z = 0$), Figure 2[B] shows that $R_{\text{SF}} \approx 4 - 12 M_\odot \text{ yr}^{-1}$, typically far lower (except for the lowest stellar-mass galaxies) than R_{SF} for

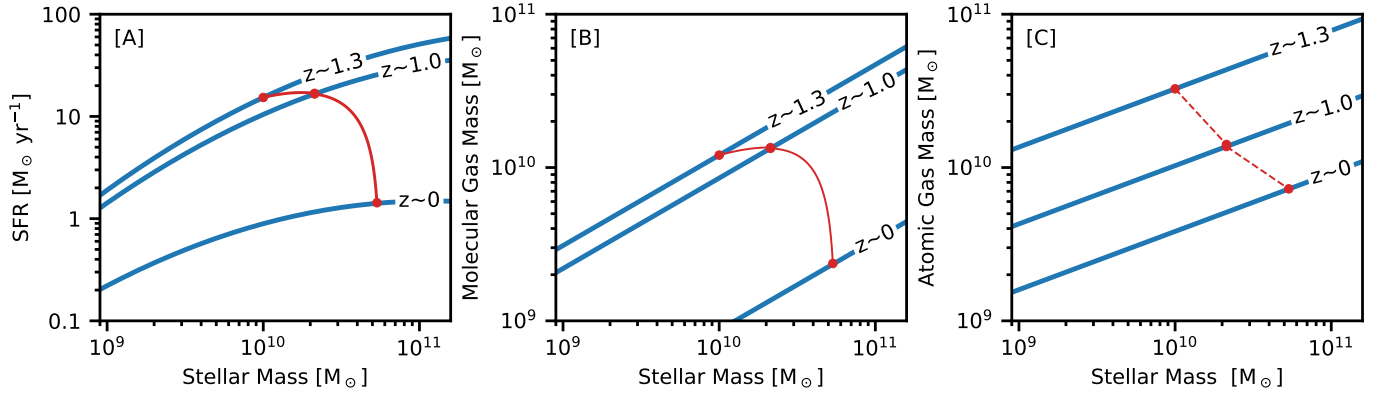


Figure 1. The panels show (in blue), as a function of stellar mass, [A] the SFR (Section 2.2), [B] the molecular gas mass (Section 2.3), and [C] the atomic gas mass (Section 2.4), for main-sequence galaxies at $z \approx 0$, $z \approx 1.0$ and $z \approx 1.3$. The red curve in Panel [A] shows the evolutionary track of a galaxy with $M_* = 10^{10} M_\odot$ at $z \approx 1.3$, obtained using Equation 1. The corresponding evolution of the molecular gas mass, obtained using Equations 1 and 9, is shown in Panel [B]. Finally, the red points in Panel [C] shows the atomic gas mass of the galaxy at the three redshifts, obtained using Equation 14. Note that the $M_{\text{Atom}} - M_*$ relation of Equation 14 is not a continuous function of redshift; the dashed line in the panel is hence only for visual aid, showing a linear interpolation between the points. See main text for discussion.

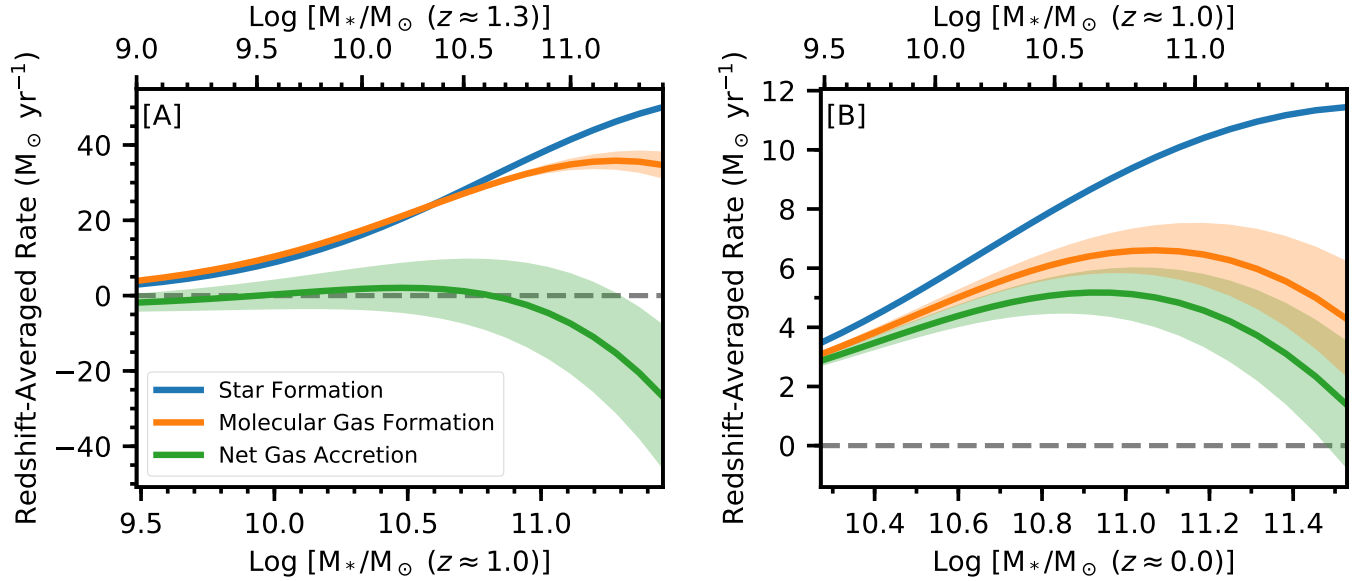


Figure 2. The two panels show the redshift-averaged star-formation rate (R_{SF} , in blue), molecular gas formation rate (R_{Mol} , in orange), and net gas accretion rate (R_{Acc} , in green) of main-sequence galaxies, as a function of the stellar mass, over [A] $z = 1.3$ to $z = 1.0$, and [B] $z = 1.0$ to $z = 0$. The shaded regions around each curve show the 68% confidence intervals. The top x-axis of panel [A] shows the initial stellar mass of the galaxies at $z = 1.3$, while the bottom x-axis shows the final stellar mass, at $z = 1.0$. This final stellar mass at $z = 1.0$ is plotted as the top x-axis of panel [B], with the bottom axis of the panel showing the final stellar mass of the galaxies at $z = 0$. The evolution of the stellar masses was obtained using Equation 1. Panel [A] shows that the molecular gas formation rate and star-formation rates are similar for all but the most massive galaxies over the interval $z = 1.3$ to $z = 1.0$, but the net gas accretion rate over the same period is much lower than the other two rates. Panel [B] shows that both the average molecular gas formation rate and the average net gas accretion rate are lower than the average SFR for the lower-redshift interval, $z = 1.0$ to $z = 0$, for galaxies of all stellar masses. See main text for discussion.

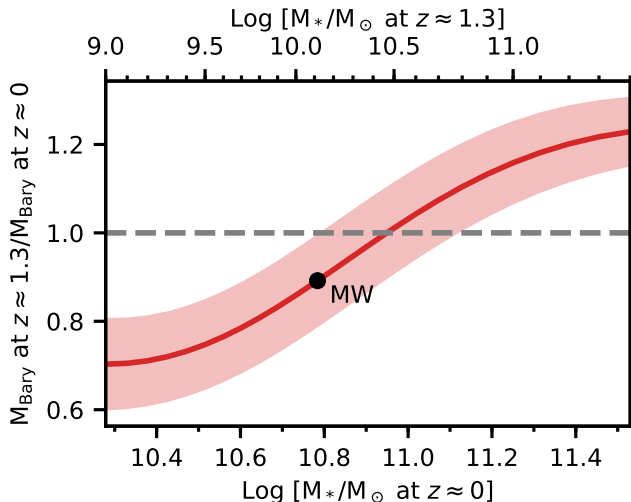


Figure 3. The ratio of the baryonic mass of main-sequence galaxies at $z \approx 1.3$ to that at $z = 0$, as a function of their stellar mass at $z \approx 0$. The black dot indicates the position on the relation of a galaxy with the stellar mass of the Milky Way today. The dashed horizontal line is at a ratio of 1, indicating no change in the baryonic mass between $z = 1.3$ and $z = 0$. It is clear that the highest-mass ($M_* \gtrsim 10^{10.5} M_\odot$ at $z \approx 1.3$) galaxies had the bulk of their baryonic mass in place by $z \approx 1.3$; the baryonic mass of these galaxies has declined over the past ≈ 9 Gyr. Conversely, the baryonic mass of galaxies with stellar mass $M_* \lesssim 10^{10} M_\odot$ at $z \approx 1.3$ has increased since $z \approx 1.3$, by approximately 30% for galaxies with $M_* \approx 10^9 M_\odot$ at $z \approx 1.3$.

the same galaxy in the higher redshift interval, $z = 1.3$ to $z = 0$. This is a direct consequence of the redshift evolution of the main-sequence relation (e.g. Whitaker et al. 2014; Popesso et al. 2022). Further, it can be seen from the figure that R_{Mol} is lower than R_{SF} for galaxies over the entire stellar-mass range. This is different from the behavior in the higher-redshift interval, where Figure 2[A] shows that $R_{\text{Mol}} \approx R_{\text{SF}}$ for all, except the most massive, galaxies. Finally, we find that the net average gas accretion rate of main-sequence galaxies over the lower redshift interval is comparable to R_{Mol} for galaxies with $M_* \gtrsim 10^{10.4} M_\odot$ today; however, R_{Acc} continues to be lower than the average SFR, especially for galaxies today with stellar masses similar to or larger than that of the Milky Way.

3.3. The Build-up of Baryons in Main-Sequence Galaxies over the past ≈ 9 Gyr

Our formalism can be used to track the build-up of baryons in galaxies³ from $z \approx 1.3$ to the present epoch. For this, we combine the estimates of the stellar mass, molecular gas mass, and atomic gas mass to estimate the baryonic mass of main-sequence galaxies at $z \approx 1.3$, $z \approx 1$, and $z \approx 0$.

³ We emphasize that this does *not* include the baryons in the CGM.

Again, we emphasize that we assume that the ionized gas mass within galaxies can be neglected relative to the stellar and neutral gas masses, and that we are not considering the CGM here. Figure 3 shows, as a function of the stellar mass of galaxies today, the fraction of the baryonic mass in individual galaxies today that was already within the galaxy by $z \approx 1.3$. It can be seen that most of the baryonic mass in star-forming galaxies with $M_* \gtrsim 10^9 M_\odot$ at $z \approx 1.3$ was already in place by $z \approx 1.3$. Indeed, Figure 3 indicates that the baryonic mass in the disk of the most massive galaxies, with $M_* \gtrsim 10^{10.4} M_\odot$ at $z \approx 1.3$, has actually *declined over the past ≈ 9 Gyr*, by $\approx 20\%$ in galaxies with $M_* \gtrsim 10^{11} M_\odot$ at $z \approx 1.3$. The bulk of the evolution in massive galaxies over the last ≈ 9 Gyr thus appears to involve the conversion of the baryonic material from atomic gas to molecular gas, and thence to stars, rather than acquisition of fresh gas from the CGM. Conversely, gas accretion from the CGM continues to play an important role in the evolution of low stellar-mass galaxies, with $M_* \lesssim 10^{10} M_\odot$ at $z \approx 1.3$. Such galaxies have acquired significant amounts of baryonic material from the CGM over the past ≈ 9 Gyr, with the largest fractional increase in the baryonic mass ($\approx 30\%$) taking place in the lowest stellar-mass galaxies, with $M_* \approx 10^9 M_\odot$ at $z \approx 1.3$.

4. DISCUSSION

Our results show that the net average gas accretion rate in main-sequence galaxies is lower than the average SFR in both redshift intervals, $z = 1.3$ to $z = 1.0$, and $z = 1.0$ to $z = 0$. This implies that the gas accretion rate does not keep pace with the SFR in main-sequence galaxies at $z \lesssim 1.3$: the star-formation activity in such galaxies is driven by the HI that is present in their disks from earlier times. Our results thus suggest that the net gas accretion was significantly more efficient at high redshifts, $z \gtrsim 1.3$, causing the build-up of HI in the disks of main-sequence galaxies. It is plausible that this efficient accretion is via the cold mode, with gas flowing along filaments onto the disks of galaxies (e.g. Kereš et al. 2005; Dekel et al. 2009). In this scenario, the large HI reservoirs resulted in a very efficient conversion of HI to H_2 at $z \approx 1 - 3$, consistent with our estimate of a high R_{Mol} , comparable to R_{SF} , over $z \approx 1.3 - 1.0$. This efficient HI-to- H_2 conversion, in turn, triggers the high star-formation activity in galaxies at these redshifts, resulting in the observed era of high star-formation activity over $z \approx 1 - 3$, the epoch of galaxy assembly (Madau & Dickinson 2014).

At later times, $z \lesssim 1.3$, a combination of physical processes are likely to have led to the observed low net gas accretion rate of Figure 2[B]. These include a transition to inefficient hot-mode accretion in massive galaxies, due to the increase in the masses of their dark matter halos (e.g. Dekel & Birnboim 2006), an increased efficiency of stellar- and AGN-driven outflows in massive galaxies that remove gas

from galaxies (e.g. Weiner et al. 2009; Veilleux et al. 2020), interactions between neighbouring galaxies that disrupt the smooth cold-mode filamentary flows, etc. The low net gas accretion rate at $z \lesssim 1.3$, combined with the very high SFR and high molecular gas formation rate, implies that the HI reservoir is consumed on a very short timescale of $\lesssim 1$ Gyr (Chowdhury et al. 2022b). This results in a decline in the average HI content of galaxies by $z \approx 1$ (Chowdhury et al. 2022d), and in a lower average molecular gas formation rate at later times, as seen in Figure 2[B] at $z < 1$. The resulting decline in the amount of molecular gas available for star formation causes a decline in the star-formation activity in individual galaxies, especially in the more massive systems that dominate the SFR density of the Universe at $z \gtrsim 1$. *The low net gas accretion rate at $z \lesssim 1.3$ is thus the primary cause of the observed decline in the SFR density of the Universe at $z \lesssim 1$.* We emphasize that the above scenario is consistent with the measurements of the large HI and H₂ reservoirs of main-sequence galaxies at $z \gtrsim 1$, and the decline in the neutral-gas content of these galaxies at later times (Chowdhury et al. 2022d,b,a; Tacconi et al. 2020).

Our estimates of R_{SF} , R_{Mol} , and R_{Acc} over $z \approx 0 - 1$ are the time-averaged rates over a relatively long, ≈ 8 Gyr, interval. This implies that there could be significant evolution in each of these quantities between $z \approx 1$ and $z \approx 0$ that is not captured by the averages in Figure 2[B]. Indeed, Bera et al. (2023a) apply a similar formalism to find that galaxies over the last ≈ 4 Gyr, from $z \approx 0.35$ to $z \approx 0$, have $R_{\text{Acc}} \approx R_{\text{SF}}$, while R_{Mol} is lower than the other two⁴. They hence conclude that the decline in the star-formation activity over the past ≈ 4 Gyr is primarily due to inefficient conversion of HI to H₂ (Bera et al. 2023a). Combining the two results, it then appears that for the first few Gyrs after $z \approx 1$, the star-formation activity continues to be limited by the accretion of HI onto galaxies, but at later times, even though the relatively low SFRs of galaxies are now comparable to their gas accretion rates, the star-formation activity continues to decline, but now primarily due to the low molecular gas formation rate. However, we caution that the ranges of stellar mass explored in the study of Bera et al. (2023a) and this work are very different, with the typical stellar masses here being far higher than those in Bera et al. (2023a). In addition, as pointed out by Bera et al. (2023a), the small cosmic volume covered in their study implies that their $M_{\text{HI}} - M_*$ scaling

relation may be affected by cosmic variance.

5. SUMMARY

In this Letter, we have combined our measurement of the $M_{\text{HI}} - M_*$ scaling relation in main-sequence galaxies at $z \approx 0.74 - 1.45$ from the GMRT-CATz1 survey, with estimates of the main-sequence relation and the $M_{\text{Mol}} - M_*$ relation, and the assumption of the continuity of main-sequence evolution, to determine the net average gas accretion rate and the molecular gas formation rate in main-sequence galaxies over two interesting intervals, $z = 1.3$ to $z = 1.0$, at the end of the epoch of galaxy assembly, and $z = 1.0$ to $z = 0$, the period when the SFR density of the Universe declines by an order of magnitude. We find that the average molecular gas formation rate is comparable to the average SFR in the former interval, but that the net gas accretion rate is significantly lower than both R_{Mol} and R_{SF} . The low net gas accretion rate results in a depletion of the HI reservoir in massive galaxies by $z \approx 1$, and causes the decline in the SFR density of the Universe at lower redshifts. In the lower-redshift interval, both R_{Acc} and R_{Mol} are lower than R_{SF} for all stellar masses; this results in the consumption of both the HI and H₂ reservoirs, and a continuing decline in the SFR density of the Universe down to the present epoch. We also find that most of the baryonic contents of massive main-sequence galaxies, with $M_* \gtrsim 10^{10.5} M_{\odot}$ at $z \approx 1.3$, was already in place ≈ 9 Gyr ago, while low-mass galaxies, with $M_* \lesssim 10^{10} M_{\odot}$ at $z \approx 1.3$, have built up approximately 30% of their baryonic content over this period.

1 We thank an anonymous referee for a report that improved
2 the clarity of this paper. We also thank the staff of the GMRT
3 who have made these observations possible. The GMRT is
4 run by the National Centre for Radio Astrophysics of the
5 Tata Institute of Fundamental Research. AC and NK thank
6 Apurba Bera for many discussions about HI scaling relations
7 and gas accretion that have contributed to this work. NK
8 acknowledges support from the Department of Science and
9 Technology via a Swarnajayanti Fellowship (DST/SJF/PSA-
10 01/2012-13). AC, NK, & JNC also acknowledge the Depart-
11 ment of Atomic Energy for funding support, under project
12 12-R&D-TFR-5.02-0700.

Software: astropy (Astropy Collaboration et al. 2013)

REFERENCES

- Astropy Collaboration, Robitaille, T. P., Tollerud, E. J., et al. 2013, A&A, 558, A33, doi: [10.1051/0004-6361/201322068](https://doi.org/10.1051/0004-6361/201322068)
- Barnes, D. G., Staveley-Smith, L., de Blok, W. J. G., et al. 2001, MNRAS, 322, 486, doi: [10.1046/j.1365-8711.2001.04102.x](https://doi.org/10.1046/j.1365-8711.2001.04102.x)

⁴ We note, for ease of comparison, that Figure 4 of Bera et al. (2023a) shows the rate of change of the molecular gas content of galaxies, i.e. $(M_{\text{Mol},f} - M_{\text{Mol},i})/\Delta t \equiv (R_{\text{Mol}} - R_{\text{SF}})$, rather than R_{Mol} as defined in Equation 4; similar conclusions are reached using either metric.

- Bera, A., Kanekar, N., Chengalur, J. N., & Bagla, J. S. 2019, *ApJL*, 882, L7, doi: [10.3847/2041-8213/ab3656](https://doi.org/10.3847/2041-8213/ab3656)
- . 2022, *ApJL*, 940, L10, doi: [10.3847/2041-8213/ac9d32](https://doi.org/10.3847/2041-8213/ac9d32)
- . 2023a, *ApJL*, 956, L15, doi: [10.3847/2041-8213/acf71a](https://doi.org/10.3847/2041-8213/acf71a)
- . 2023b, *ApJL*, 950, L18, doi: [10.3847/2041-8213/acd0b3](https://doi.org/10.3847/2041-8213/acd0b3)
- Bothwell, M. S., Maiolino, R., Kennicutt, R., et al. 2013, *MNRAS*, 433, 1425, doi: [10.1093/mnras/stt817](https://doi.org/10.1093/mnras/stt817)
- Bouché, N., Dekel, A., Genzel, R., et al. 2010, *ApJ*, 718, 1001, doi: [10.1088/0004-637X/718/2/1001](https://doi.org/10.1088/0004-637X/718/2/1001)
- Catinella, B., Saintonge, A., Janowiecki, S., et al. 2018, *MNRAS*, 476, 875, doi: [10.1093/mnras/sty089](https://doi.org/10.1093/mnras/sty089)
- Chengalur, J. N., Braun, R., & Wieringa, M. 2001, *A&A*, 372, 768, doi: [10.1051/0004-6361:20010547](https://doi.org/10.1051/0004-6361:20010547)
- Chowdhury, A., Kanekar, N., & Chengalur, J. N. 2022a, *ApJL*, 935, L5, doi: [10.3847/2041-8213/ac8150](https://doi.org/10.3847/2041-8213/ac8150)
- . 2022b, *ApJ*, 937, 103, doi: [10.3847/1538-4357/ac7d52](https://doi.org/10.3847/1538-4357/ac7d52)
- . 2022c, *ApJL*, 941, L6, doi: [10.3847/2041-8213/ac9d8a](https://doi.org/10.3847/2041-8213/ac9d8a)
- . 2022d, *ApJL*, 931, L34, doi: [10.3847/2041-8213/ac6de7](https://doi.org/10.3847/2041-8213/ac6de7)
- Chowdhury, A., Kanekar, N., Chengalur, J. N., Sethi, S., & Dwarakanath, K. S. 2020, *Nature*, 586, 369, doi: [10.1038/s41586-020-2794-7](https://doi.org/10.1038/s41586-020-2794-7)
- Chowdhury, A., Kanekar, N., Das, B., Dwarakanath, K. S., & Sethi, S. 2021, *ApJL*, 913, L24, doi: [10.3847/2041-8213/abfcc7](https://doi.org/10.3847/2041-8213/abfcc7)
- Daddi, E., Bournaud, F., Walter, F., et al. 2010, *ApJ*, 713, 686, doi: [10.1088/0004-637X/713/1/686](https://doi.org/10.1088/0004-637X/713/1/686)
- Dekel, A., & Birnboim, Y. 2006, *MNRAS*, 368, 2, doi: [10.1111/j.1365-2966.2006.10145.x](https://doi.org/10.1111/j.1365-2966.2006.10145.x)
- Dekel, A., Birnboim, Y., Engel, G., et al. 2009, *Nature*, 457, 451, doi: [10.1038/nature07648](https://doi.org/10.1038/nature07648)
- Dénes, H., Kilborn, V. A., & Koribalski, B. S. 2014, *MNRAS*, 444, 667
- Giovanelli, R., Haynes, M. P., Kent, B. R., et al. 2005, *AJ*, 130, 2598, doi: [10.1086/497431](https://doi.org/10.1086/497431)
- Huang, S., Haynes, M. P., Giovanelli, R., & Brinchmann, J. 2012, *ApJ*, 756, 113, doi: [10.1088/0004-637X/756/2/113](https://doi.org/10.1088/0004-637X/756/2/113)
- Kalberla, P. M. W., & Kerp, J. 2009, *ARA&A*, 47, 27, doi: [10.1146/annurev-astro-082708-101823](https://doi.org/10.1146/annurev-astro-082708-101823)
- Kereš, D., Katz, N., Weinberg, D. H., & Davé, R. 2005, *MNRAS*, 363, 2, doi: [10.1111/j.1365-2966.2005.09451.x](https://doi.org/10.1111/j.1365-2966.2005.09451.x)
- Leitner, S. N. 2012, *ApJ*, 745, 149, doi: [10.1088/0004-637X/745/2/149](https://doi.org/10.1088/0004-637X/745/2/149)
- Leitner, S. N., & Kravtsov, A. V. 2011, *ApJ*, 734, 48, doi: [10.1088/0004-637X/734/1/48](https://doi.org/10.1088/0004-637X/734/1/48)
- Madau, P., & Dickinson, M. 2014, *ARA&A*, 52, 415, doi: [10.1146/annurev-astro-081811-125615](https://doi.org/10.1146/annurev-astro-081811-125615)
- Møller, P., Fynbo, J. P. U., Ledoux, C., & Nilsson, K. K. 2013, *MNRAS*, 430, 2680, doi: [10.1093/mnras/stt067](https://doi.org/10.1093/mnras/stt067)
- Noeske, K. G., Weiner, B. J., Faber, S. M., et al. 2007, *ApJL*, 660, L43, doi: [10.1086/517926](https://doi.org/10.1086/517926)
- Parkash, V., Brown, M. J. I., Jarrett, T. H., & Bonne, N. J. 2018, *ApJ*, 864, 40, doi: [10.3847/1538-4357/aad3b9](https://doi.org/10.3847/1538-4357/aad3b9)
- Peng, Y.-j., Lilly, S. J., Kovač, K., et al. 2010, *ApJ*, 721, 193, doi: [10.1088/0004-637X/721/1/193](https://doi.org/10.1088/0004-637X/721/1/193)
- Péroux, C., & Howk, J. C. 2020, *ARA&A*, 58, 363, doi: [10.1146/annurev-astro-021820-120014](https://doi.org/10.1146/annurev-astro-021820-120014)
- Popesso, P., Concas, A., Cresci, G., et al. 2022, *MNRAS*, doi: [10.1093/mnras/stac3214](https://doi.org/10.1093/mnras/stac3214)
- Renzini, A. 2009, *MNRAS*, 398, L58, doi: [10.1111/j.1745-3933.2009.00710.x](https://doi.org/10.1111/j.1745-3933.2009.00710.x)
- Rodighiero, G., Daddi, E., Baronchelli, I., et al. 2011, *ApJL*, 739, L40, doi: [10.1088/2041-8205/739/2/L40](https://doi.org/10.1088/2041-8205/739/2/L40)
- Saintonge, A., & Catinella, B. 2022, arXiv e-prints, arXiv:2202.00690. <https://arxiv.org/abs/2202.00690>
- Saintonge, A., Catinella, B., Tacconi, L. J., et al. 2017, *ApJS*, 233, 22, doi: [10.3847/1538-4365/aa97e0](https://doi.org/10.3847/1538-4365/aa97e0)
- Santini, P., Maiolino, R., Magnelli, B., et al. 2014, *A&A*, 562, A30, doi: [10.1051/0004-6361/201322835](https://doi.org/10.1051/0004-6361/201322835)
- Scoville, N., Sheth, K., Aussel, H., et al. 2016, *ApJ*, 820, 83, doi: [10.3847/0004-637X/820/2/83](https://doi.org/10.3847/0004-637X/820/2/83)
- Scoville, N., Lee, N., Vanden Bout, P., et al. 2017, *ApJ*, 837, 150, doi: [10.3847/1538-4357/aa61a0](https://doi.org/10.3847/1538-4357/aa61a0)
- Speagle, J. S., Steinhardt, C. L., Capak, P. L., & Silverman, J. D. 2014, *ApJS*, 214, 15, doi: [10.1088/0067-0049/214/2/15](https://doi.org/10.1088/0067-0049/214/2/15)
- Tacconi, L. J., Genzel, R., & Sternberg, A. 2020, *ARA&A*, 58, 157, doi: [10.1146/annurev-astro-082812-141034](https://doi.org/10.1146/annurev-astro-082812-141034)
- Tacconi, L. J., Neri, R., Genzel, R., et al. 2013, *ApJ*, 768, 74, doi: [10.1088/0004-637X/768/1/74](https://doi.org/10.1088/0004-637X/768/1/74)
- Veilleux, S., Maiolino, R., Bolatto, A. D., & Aalto, S. 2020, *A&A Rv*, 28, 2, doi: [10.1007/s00159-019-0121-9](https://doi.org/10.1007/s00159-019-0121-9)
- Walter, F., Carilli, C., Neeleman, M., et al. 2020, *ApJ*, 902, 111, doi: [10.3847/1538-4357/abb82e](https://doi.org/10.3847/1538-4357/abb82e)
- Weiner, B. J., Coil, A. L., Prochaska, J. X., et al. 2009, *ApJ*, 692, 187, doi: [10.1088/0004-637X/692/1/187](https://doi.org/10.1088/0004-637X/692/1/187)
- Whitaker, K. E., Franx, M., Leja, J., et al. 2014, *ApJ*, 795, 104, doi: [10.1088/0004-637X/795/2/104](https://doi.org/10.1088/0004-637X/795/2/104)
- Zwaan, M. A. 2000, PhD thesis, Ph.D. Thesis, Groningen: Rijksuniversiteit, 2000